Environ Monit Assess (2018) 190:348
https://doi.org/10.1007/s10661-018-6689-0

Determining representative ranges of point sensors in distributed networks

John K. Horne · Dale A. Jacques II

Received: 17 August 2017 / Accepted: 16 April 2018

Abstract Distributed networks of stationary instruments provide high temporal scope (i.e., range/resolution) observations but are spatially limited as a set of point measurements. Measurement similarity between points typically decays with distance, which is used to set interpolation distances. The importance of analyzing spatiotemporal data at equivalent spatial and temporal scales has been identified but no standard procedure is used to interpolate space using temporally-indexed observations. Using concurrent mobile and stationary active acoustic, fish density data from a tidal energy site in Puget Sound, WA, USA, six methods are compared to estimate the range at which stationary measurements can be spatially interpolated. Four methods estimate the representative range of the mean using autocorrelation or paired *t*-test and repeated measures ANOVA. Accuracy of resulting sensor density estimates was modeled as departures from interpolated linear and aerial estimates. Two methods were used to estimate representative range of the variance by comparing theoretical spectra or by determining equivalent spatial and temporal scales. Representative ranges of means extended from 30.57 to 403.9 m. Estimation error (i.e., standard deviation) ranges of linearly interpolated or aerially extrapolated values ranged from 42.5 to 82.3%. Representative ranges using variance measurements differed by a factor of approximately two (scale equivalence = 648.7 m, theoretical = 1388.1 m). A six-step decision tree is presented to guide identification of monitoring variables and choice of method to calculate representative ranges in distributed networks. This approach is applicable for networks of any size, in aquatic or terrestrial environments, and monitoring the mean or variance of any quantity.

Keywords Distributed networks · Representative range · Point sensors · Spatial representativeness

J. K. Horne (✉) · D. A. Jacques II,
School of Aquatic and Fishery Sciences, University of Washington, Box 355020, Seattle, WA 98195, USA
e-mail: jhorne@uw.edu

Present Address:
D. A. Jacques
Procured Health, 33 N. LaSalle Suite 1500, Chicago, IL 60602, USA

Introduction

When monitoring aquatic ecosystems, samples are traditionally collected from mobile (e.g., survey vessels) and/or fixed (e.g., moorings, bottom-mounted packages) platforms. Samples can be discrete or continuous measurements that are used to detect change in relevant quantities over space and/or time. Technological advances in sensor design, computer processing, data storage, and data management (e.g., Godø et al. 2014) have increased the number of biological and physical variables that can be measured from integrated networks of point-source sensors (i.e., fixed platforms). Point-source sensor networks (e.g., Porter et al. 2005) typically increase deployment times relative to vessel-based,

Published online: 18 May 2018

mobile surveys and are assumed more cost-effective for long-term measurements due to reduced labor and ship-time costs. This assumption may evolve as an increasing number of surface and subsurface autonomous, mobile platforms (e.g., sail drone, sea gliders) are available to spatially sample over extended periods (i.e., months).

Challenges associated with drawing spatial inferences from point-source measurements include identifying what area a sample represents and quantifying measurement uncertainty when interpolating measurements between or among sensors. Biological similarity, measured as community composition, density, or distribution, typically decays with distance due to spatial heterogeneity in physical habitats (Nekola and White 1999), biological aggregation (Roughgarden 1977), predation (Wiens 1976), and patchiness produced by environmental constraints on organismal dispersal (Garcillán and Ezcurra 2003) or physiological limitations (e.g., Hubbell 2001). Measurement uncertainty is related to the rate at which quantities change with time and/or distance from an initial measurement (e.g., Ellis and Schneider 1997). One consequence of distance decay is that the correlation between two samples decreases with increasing distance until the correlation approaches zero, and meaningful inferences about a second sample can no longer be derived from the first. This distance represents the range of independent samples. Interpolation of point measurements beyond this radius increases uncertainty and interpretation errors (Anttila et al. 2008; Martin et al. 2005; Milewska and Hogg 2001). From a sampling optimization perspective, additional measurements collected within this radius are sub-optimal and the effort could be used to increase the range of a survey. Rooted in Tversky and Kahneman's (1975) psychological concept of "representativeness heuristics," the maximum distance to which point measurements can be used to resolve spatial variability in a surrounding domain (i.e., defined area) is termed the "spatial representativeness" of a point sample (Janis and Robeson 2004). To avoid the wrath of our English teachers who forbade the use of derivational suffixes (i.e., "ness monsters"), we will use the term representative range rather than "spatial representativeness."

Representative range is not a new concept. It was first used in meteorology to optimize the spatial coverage of rain gauges and other meteorological sensors (Brooks 1947; Huff and Neill 1957). Early studies of meteorological network design focused on identifying the number of randomly placed rain gauges to achieve a predetermined accuracy of mean rainfall in a spatial domain (e.g., Rycroft 1949). It was soon realized that optimum sensor density is dependent on the quantity being measured and the measurement objective (e.g., rainfall fore- or hindcasting) of a network (Brooks 1947). Spatial autocorrelation influences the representative range of sensors, which shifted research effort from determining the number of required sensors, to determining the distance or range between sensors (e.g., Hershfield 1965; Hutchinson 1969, 1970). Network optimization efforts also shifted from determining the spatial autocorrelation between sensors to quantifying the relative error introduced by interpolating among points (Gandin 1970) or areas (Kagan 1966). Since the 1970s, representative range studies diversified to focus on the effects of spatial and temporal binning (Ciach and Krajewski 2006) and methods of post hoc network optimization such as cluster analysis (e.g., Sulkava et al. 2011) and variogram nugget time series (e.g., Janis and Robeson 2004). Despite these advances, many network optimization methods proposed in the 1960s and 1970s are still used to optimize the design of meteorological networks (e.g., Milewska and Hogg 2001; Ciach and Krajewski 2006).

Few ecological studies have examined relationships between community structure and designs of stationary sensor networks (Rhodes and Jonzén 2011), despite extensive efforts to characterize relationships among ecological quantities through time and over space (Legendre 1993; Posadas et al. 2006; Soininen et al. 2007). Given that the deployment and operation of sensor networks are typically resource limited, several studies have quantified the optimal spatial and temporal allocation of sampling effort based on the perceived or known spatiotemporal variability within a domain (e.g., Gray et al. 1992; Kitsiou et al. 2001; Rhodes and Jonzén 2011), or have optimized sensor allocation within networks (e.g., Siljamo et al. 2008). The challenge when designing stationary sensor networks is to determine the number of sensors that are needed to meet sampling objectives. This paper shifts the focus of network design from, "How many sensors can we afford?" to "How many sensors do we need to meet our objective(s)?"

We used concurrent mobile and stationary data to investigate the potential of six methods to *a priori* define representative ranges for sensors in a distributed, stationary network. This approach contrasts to most modern techniques that use post hoc optimization (e.g., Janis and Robeson 2004; Sulkava et al. 2011) for the same purpose. The feasibility of each method is evaluated

using a case study that was designed to acoustically monitor fish densities at a Marine Renewable Energy (MRE) tidal site in Puget Sound, WA, USA.

Methods

In this section, the theory, algorithms, and approach will be described for the six methods used to calculate representative ranges. Details of the case study site and sampling follow method descriptions.

Calculating representative ranges

Six methods were chosen to quantify the representative range of temporal, point measurements (Table 1). Four of these methods estimate the representative range of the mean of a monitoring metric, while the remaining two estimate the representative range of the metric variance. The six methods mirror the evolution of techniques used to optimize meteorological sensor networks and can broadly be categorized in four approaches: distance between sensors based on spatial correlation; sample size calculations assuming random sampling to detect a minimum threshold of change; maximization of spatial variance; and equivalent scales of spatial and temporal variability.

The first approach calculates the optimum distance between sensors based on the relationship of spatial measurements. Using the decay of spatial autocorrelation with distance (e.g., Anttila et al. 2008), the range at which measurements become independent is set as the representative range. This method evolved in the mid- to late 1960s in meteorology (Hershfield 1965) and has the most widespread acceptance in biological or ecological studies (e.g., Jacobs 1989; Anttila et al. 2008). Spatial autocorrelation models of representative range evolved to models of interpolation error (e.g., Kagan 1966; Gandin 1970; Milewska and Hogg 2001). Lacking a meaningful error threshold to determine representative range, interpolation error was traditionally used to quantify the uncertainty within each method. In this study, interpolation error curves for linear and areal interpolation are used to quantify error for the four methods used to quantify representative ranges of the mean.

The second approach quantifies the number of sensors needed to detect change using paired samples evaluated with *t*-tests in sample size calculations. Assuming that random sampling will identify biological change (e.g., Rycroft 1949), point samples are used before and after a perturbation. Three methods use this random sampling approach: the number of replicates using a derivative of minimum sample size calculations for a paired *t*-test (Gray et al. 1992), a paired *t*-test/repeated measures ANOVA (Sullivan 2006), and a sample size calculation for a paired *t*-test including statistical power (Zar 2010).

Although changes in temporal variance can be used as a metric of biological change (Underwood 1991), there is no reason to assume that the temporal variance of a series matches the spatial structure of the mean (e.g., Certain et al. 2007; Damian et al. 2003; Sampson et al. 2001). The third approach models the theoretical power spectrum of a temporal series as a function of the spatial autocorrelation model developed for the second approach. Point measurements of temporal variance have an equivalent spatial range over which they can be interpolated (i.e., spatial period). The spatial period where 95% of the maximum variance in fish density was observed is set as the representative range of the variance.

The final approach compares empirical spatial and temporal power spectra (i.e., distribution of variance in a data series as a function of frequency) to identify equivalent scales of spatial and temporal variability by identifying periods at which magnitudes of spatial and temporal variability matched.

Representative range of the mean

Spatial autocorrelation

Lagged autocorrelation functions identify representative ranges by quantifying relationships in a temporal or spatial series (Legendre 1993; Mønness and Coleman 2011). Lagged Pearson's product-moment correlation coefficients $\left(\hat{\dot{\rho}}\right)$ define the correlation between all measurements at a given lag (h), which can be simplified as the covariance $\left(\hat{C}\right)$ of measurements at lag h standardized by the variance $\left(\hat{\sigma}^2\right)$ of the series:

$$\hat{\dot{\rho}}(h) = \frac{\hat{C}(h)}{\hat{\sigma}^2} \tag{1}$$

where $\hat{C}$ is used to measure similarity. The lagged autocorrelation is the degree to which two measurements match relative to the variance in the series:

$$\hat{\dot{\rho}}(h) = \hat{\dot{\rho}}(0)e^{-\alpha d} \tag{2}$$

Table 1 Properties of six methods used to estimate representative ranges of ecological point sensors

Method	Quantity property	Spatially explicit?	Analytical approach	Origin or reference
Spatial autocorrelation	Mean	Yes	Autocorrelation	Anttila et al. (2008)
Gray's sample size calculation	Mean	No	Paired *t*-test/repeated measures ANOVA	Gray et al. (1992)
T-test sample size calculation	Mean	No	Paired *t*-test/repeated measures ANOVA	Sullivan (2006)
T-test power analysis	Mean	No	Paired *t*-test/repeated measures ANOVA	Zar (2010)
Theoretical spectra	Variance	Indirectly	Modeled spatial power spectra	Gilman et al. (1962)
Equivalent spatial and temporal scales	Variance	Indirectly	Empirical spatial and temporal power spectra	Wiens (1989)

where $\hat{\rho}(0)$ is the autocorrelation at a spatial or temporal lag of 0, d is the number of lags, and α is the range at which the autocorrelation decays by a value of e (i.e., inverse scale height, Kagan 1972). In theory, $\hat{\rho}(0)$ should equal unity, indicating a perfect autocorrelation at lag 0. In practice, these lags often deviate from unity due to variability at scales below the sampling resolution (g) that cannot be resolved (i.e., nugget effect). Lagged correlation coefficients are used to estimate biological patch sizes (e.g., Legendre 1993) and to determine sampling resolutions that do not violate statistical assumptions of independence (Schneider 1990). The squared correlation coefficient is mathematically identical to the coefficient of determination (R^2), both of which quantify the proportion of variability attributed to spatial correlation.

Assuming a random series, lagged correlation coefficients are distributed around zero with a variance of $1/n$, with n bins equaling the length of the data series. Assuming a random distribution, the length of the 95% confidence interval of lagged correlation coefficients is $2/\sqrt{l}$, where l is the number of lags in the series. Substituting $2/\sqrt{l}$ for $\hat{\rho}(h)$ in Eq. 2, the representative range (r_{rep}) is the range given by the number lags (d) of resolution or grain size g:

$$r_{\text{rep}} = -g\left(\frac{ln\left(\frac{\left(\frac{2}{\sqrt{l}}\right)^2}{\hat{\rho}(0)}\right)}{\alpha}\right) \tag{3}$$

A coefficient of determination model was used to describe how similarity in fish density decayed over distance in the Admiralty Inlet case study. Lagged Pearson's correlation coefficients were calculated using backscatter data from each surface transect ($n = 547$), then squared to create lagged coefficients of determination (R^2). An exponential decay model was fit across all transects to the lagged correlation coefficients and coefficients of determination using a least squares algorithm. Once the range was determined, the representative area was defined by a circle with a radius equal to the representative range. Representative range areas from the corresponding circle were then standardized to a square kilometer and used to calculate the density of sampling packages required within the sampling domain.

Random sampling size

Gray et al. (1992) determined the number of stations n needed to detect a difference in community abundance at temporal lag t when optimizing spatial sampling effort and sample allocation. Sampling effort is determined by:

$$n = \frac{s^2}{\text{RPE}^2\bar{x}^2} \tag{4}$$

where s and $\bar{x}$ are the standard deviation and mean of samples in a pilot study, and the Relative Percent Error (RPE) is the minimum error as a proportion of the mean. In an alternate approach, Sullivan (2006) used a derivative of the sample size calculation (Eq. 4) in a repeated measures ANOVA for detecting the mean difference in paired means, calculated from measurements paired through time:

$$n_{\text{pairs}} = \left(\frac{Z_{1-\alpha/2} * \sigma_d}{E}\right)^2 \tag{5}$$

The Z-score critical value for a two-tailed test, $Z_{1-\alpha/2}$, at $\alpha = 0.05$ (i.e., 0.95 significance level) is 1.96. σ_d is the standard deviation of the paired differences between times at each station. The variance of differences between normal distributions is the sum of both variances. Assuming variance remains constant through time, σ_d can be expressed as:

$$\sigma_d = \sqrt{2*\sigma_t^2} \tag{6}$$

where σ_t^2 is the spatial variance at time t. If Eq. 4 is a derivative of Eq. 5, then Eq. 4 underestimates the required sample size by a factor of $\left(Z_{1-\alpha/2}\right)^2$, (=3.84 if $\alpha = 0.05$) by not including the squared Z test statistic in the numerator and by another factor of 2 for not accounting for the increased variance of the normal difference distribution. E in Eq. 5 is the absolute effect size, which when standardized by the mean $\bar{x}$ produces the RPE from Eq. 4:

$$\mathrm{RPE} = \frac{E}{\bar{x}} \tag{7}$$

Given a known sampling domain S over which σ_t is measured, and assuming a relatively even distribution of sensors, the representative area a_{rep} can be can then be calculated as:

$$a_{\mathrm{rep}} = \frac{S}{n_{\mathrm{pairs}}} \tag{8}$$

Substituting Eq. 5 for n_{pairs} in Eq. 8:

$$a_{\mathrm{rep}} = \frac{S}{\left(\frac{Z_{1-\alpha/2}*\sigma_d}{\mathrm{RPE}*\bar{x}}\right)^2} \tag{9}$$

The representative range corresponds to the radius r_{rep} of the circle defined in a_{rep}:

$$a_{\mathrm{rep}} = \pi r_{\mathrm{rep}}^2 \tag{10}$$

which can be combined with Eq. 9:

$$r_{\mathrm{rep}} = \sqrt{\frac{S}{\pi*\left(\frac{Z_{1-\alpha/2}*2\sigma_t}{\mathrm{RPE}*\bar{x}}\right)^2}} \tag{11}$$

Equation 11 is used to avoid type I errors associated with a false positive test.

Power analysis calculations can also be used to identify the sample size required to identify changes with adequate statistical power (Zar 2010). The required number of pairs in a paired t-test power analysis is:

$$n_{\mathrm{pairs}} = \frac{\sigma_d^2\left(Z_{1-\alpha/2} + Z_\beta\right)^2}{E_d^2} \tag{12}$$

where σ_d^2 can be calculated following Eq. 6. Both $Z_{1-\alpha/2}$ and Z_β represent critical Z-scores corresponding to subjectively chosen α and β values. These values are commonly set to 1.96 ($\alpha = 0.05$) and 0.84 ($\beta = 0.80$) representing two standard deviations. E_d is analogous to the effect size introduced in Eq. 5. The representative range can then be calculated by substituting n_{pairs} into Eqs. 8, 9, and 10.

These methods calculate the required sample size of measurements paired through time and analyzed using a paired t-test, where the number of pairs corresponds to the number of sensors in a network. Observations are only analyzed at two distinct times, comparing undisturbed and post-perturbation measurements. T-tests assume a normal distribution of paired differences, which is satisfied if both measurement sets are normally distributed by the normality of normal difference distributions (Zar 2010). A t-test sample size calculation assumes random sampling, which treats all spatially distinct samples as random samples of the mean. Unlike autocorrelation analysis, which describes the range to which inferences can be made, the sample size calculation calculates the number of stations required to make statements about the domain, if spatial variability is treated as random variance. Sample size calculations require estimates of spatial variability, which must be acquired from spatially-indexed data. The more baseline spatially-indexed data collected, the more accurate estimates of the spatial variance become.

In the Admiralty Inlet case study, estimates of r_{rep} were calculated independently using Gray's sample size, t-test sample size, and power analysis formulas. To remove the spatial autocorrelation from the series due to non-random fish distributions (Bence 1995), sample size calculations were conducted at statistically independent resolutions over the range of the sampling grid. Sequentially sampled line-transects were used to minimize the confounding of spatial and temporal variance. The minimum acoustic effect size, E, was arbitrarily set to 1 dB, which equates to a 25.9% change in fish density. A 1 dB re $1\mathrm{m}^{-1}$ change

compared to the grand mean of − 77 dB effect size of 1 dB translates to a RPE value of 0.0129 $\left(\text{i.e.,}\left|\frac{\pm 1\text{ dB}}{-77\text{ dB}}\right|\right)$. Alpha was set at 0.05, and beta in the power analysis was conservatively set to 0.90.

Interpolation errors

Accuracy of sensor density estimates can be modeled as deviations from interpolated estimates. Sensor density can be optimized by setting the magnitude or error in the linear (Gandin 1970) or areal (Kagan 1966) interpolation. The relative standard interpolation error (RSIE) is the error introduced by interpolating point measurements to distant points or areas. When linearly interpolating between two points, the RSIE is maximized at the midpoint of the vector defined by those points. RSIE of linear interpolation (Gandin 1970) is calculated as:

$$\text{RSIE}_{\text{interpolation.point}} = \sqrt{1-\frac{2\rho^2\left(\frac{d}{2}\right)}{1+\eta+\rho(d)}} \tag{13}$$

where $\rho(d)$ is the modeled exponential decay function from Eq. 2 and η is defined as:

$$\eta = 1-\rho(0) \tag{14}$$

For an arbitrary RSIE, Eq. 13 is solved to give the maximum interpolation distance d.

Assuming that the representative area is a circle, the representative range will be the radius of a circle. The corresponding areal interpolation error (Kagan 1966) is defined as:

$$\text{RSIE}_{\text{interpolation.area}} = \sqrt{\sigma_\varepsilon^2 + 0.23\sigma_p^2\frac{\sqrt{S}}{D_0}} \tag{15}$$

where σ_p^2 is the temporal variance at the point, S is the area over which the point is interpolated, D_0 is the inverse of range α in Eq. 2, and σ_ε^2 is defined as:

$$\sigma_\varepsilon^2 = \eta\sigma_p^2 \tag{16}$$

Given a predetermined $\text{RSIE}_{\text{interpolation.area}}$ in Eq. 13, the equation can be solved for the area S, which is the area of the circle defined by radius r_{rep}:

$$S = \left(\frac{D_0\left(\text{RSIE}^2-\sigma_\varepsilon^2\right)}{0.23*\sigma_p^2}\right)^2 \tag{17}$$

and then solved for r_{rep} as a function of S, similar to Eqs. 8, 9, 10, and 11:

$$r_{\text{rep}} = \sqrt{\frac{\left(\frac{D_0\left(\text{RSIE}^2-\sigma_\varepsilon^2\right)}{0.23*\sigma_p^2}\right)^2}{\pi}} \tag{18}$$

RSIE analysis is based on exponential decay in spatial autocorrelation. Even if RSIE is not used to determine the representative range of point sensors within networks, it can be used to estimate interpolation errors. In the absence of a meaningful RSIE threshold, RSIE curves can be used to describe the error in the three representative ranges identified using correlation coefficient models (i.e., Gray's sample size calculation, t-test sample size calculations, and power analysis). RSIE analysis can be conducted for any data used to estimate autocorrelation. The only additional requirement is an estimate of the temporal variance when interpolating a point measurement to a surrounding area (see Eq. 15). Except for Eq. 15, every parameter is derived from the spatial autocorrelation, estimated using spatially-indexed data. In the Admiralty Inlet test case, temporal variance, in Eq. 15, was calculated using data from a point-source (i.e., echosounder) but could be calculated using repeated, spatially-indexed data.

Representative range of the variance

Theoretical spectra

Temporal variability of the mean varies through space in ecological quantities (Certain et al. 2007; Damian et al. 2003; Hocke and Kämpfer 2011), with high temporal variability often spatially aggregated. Point measurements used to estimate temporal variance also have a representative range.

The first technique to estimate the representative range of temporal variance is a combination of autocorrelation and spectral power (i.e., variance in a series as a function of frequency, per unit frequency). Due to autocorrelation in a series, the power spectra of a red-noise (i.e., spectral power decreases as $1/f^2$), first-order autoregressive process is minimized at small periods and increases logistically with period (Gilman et al. 1962):

$$L_f = \frac{1-\rho^2(1)}{1+\rho^2(1)-2\rho(1)\times\cos\left(\frac{2\pi\times k}{l}\right)} \tag{19}$$

where L_f is the ratio of the predicted variance relative to the variance of a random, white-noise (i.e., equal power

across frequency bands) process. Multiplying L_f by the white-noise variance produces an estimate of the true predicted variance. $\rho(1)$ is calculated by substituting 1 for d in Eq. 2. The factor of two within the cosine argument was not included in the Gilman et al. (1962) original derivation but included in subsequent applications (e.g., Torrence and Compo 1998) so that L_f approaches the maximum variance at frequencies approaching zero. In Eq. 19, l is the maximum lag distance and k/l is the frequency as a function of the maximum lag distance l. The autocorrelation at lag 1, $\rho(1)$, is first modeled in Eq. 2. At frequencies approaching zero (i.e., maximum period), the cosine term approaches zero and the maximum predicted variance in a red-noise spectrum simplifies to:

$$L_{f.\max} = \frac{1-\rho^2(1)}{1+\rho^2(1)-2\rho(1)} \tag{20}$$

The normalized variance increases logistically as a function of the first-order correlation coefficient. The scale at which the variance can be considered representative is the scale where a suitably high proportion b of the maximum variance, expressed in Eq. 20, is expected to be observed. Equation 17 can be set equal to the proportion p of the maximum predicted variance in Eq. 20 and then solved for the frequency. The inverse of the frequency is the period at which measurements of the variance are considered representative and can be calculated from Eq. 19. The frequency from Eq. 17 at which we expect to see p described in Eq. 19 is the period at which measurements of variance are considered representative. This relationship can be quantified by combining Eq. 20 and Eq. 17:

$$\overbrace{p * \left(\frac{1-\rho^2(1)}{1+\rho^2(1)-2\rho(1)}\right)}^{\text{Equation 20}} = \overbrace{\frac{1-\rho^2(1)}{1+\rho^2(1)-2\rho(1)*\cos\left(\frac{2\pi*k}{l}\right)}}^{\text{Equation 17}} \tag{21}$$

Which can be simplified to:

$$\text{period}_{\text{rep}} = \frac{l}{k} = g \times \left(\frac{2\pi}{\operatorname{acos}\left(\frac{\left(\frac{1+\rho^2(1)-2\rho(1)}{p}\right)-1-\rho^2(1)}{-2\rho(1)} \right)} \right) \tag{22}$$

Modeled power spectra assume that the scale at which the variance approaches the maxima is the scale at which the variance is representative. The only spatial parameter included in the model is the first-order autocorrelation, assuming a red-noise, random walk model.

In the Admiralty Inlet data, power spectra are modeled using the best-fit autocorrelation model previously described. This model assumes fish densities are distributed around a uniform field with first-order autocorrelation. This assumption is more easily explained as a one-dimensional time series, where the value at interval n is only dependent on the previous value and a variance Y, without any trends, covariates, or natural cycles in the data.

$$X_n = \rho(1)X_{n-1} + Y_n, \text{ for all } n \text{ lagged by distance } t \tag{23}$$

Red-noise spectra were modeled using the lagged correlation coefficients fit to an exponential decay model. The proportion of the maximum variance deemed representative p was set at 95%. The scale at which the predicted variance reached 95% of the maximum variance was calculated using Eq. 22.

Equivalent space and time scales

Although the relationship between spatial and temporal variability periods may be variable, an equivalent spatial period exists for every temporal period. Measurements of temporal variance collected from a point sensor are considered representative of spatial variability at the equivalent spatial period. Assuming linearity in the spatial and temporal power-law spectra, the variance at the largest resolvable temporal period, limited by the Nyquist frequency (i.e., a period of half the temporal series length, cf. Platt and Denman 1975), can be compared to the spatial spectra to identify the

corresponding spatial period at which equivalent amounts of variability are expected to be observed.

Wavelet analysis (Torrence and Compo 1998) was used to compare and contrast representative ranges of spatial and temporal variance in acoustic data from Admiralty Inlet. The global wavelet spectra, an averaged wavelet spectra across all instances, is analogous to the Fourier power spectra (Hudgins et al. 1993; Percival 1995; Perrier et al. 1995). Continuous wavelet transforms, which analyze periods at redundantly small intervals, were used to increase period resolution (Torrence and Compo 1998) and averaged through time:

$$w(T) = \frac{\overline{W}^2(T)}{\delta^2} = \frac{1}{N}\sum_{n=0}^{N-1} |\, W_n(T)|^2 \tag{24}$$

where $\overline{W}^2$ is the mean wavelet power and T is the bandwidth over which wavelet powers are averaged over n times to N length. Spatial and temporal scales were resolved using 12 steps per octave, a common period resolution in ecological contexts (Urmy et al. 2012), from twice the resolution of the series to the Nyquist frequency as:

$$\underset{2g\rightarrow \text{Nyquist}}{T} = g \times 2^{(i+11)/12} \tag{25}$$

where g is the spatial or temporal resolution of the measurement, and the maximum scale is limited by half the extent of the series (i.e., Nyquist frequency; Platt and Denman 1975). Wavelets were decomposed using a Morlet wavelet of frequency 6, with a known dilation of 1.03 to translate the wavelet scale to the equivalent Fourier power spectra period (Torrence and Compo 1998). Potential bias from peaks in the global wavelet spectrum was not corrected as the bias is a uniform factor of the wavelet scale in both the spatial and temporal density series (Liu et al. 2007).

In the Admiralty Inlet data, the global wavelet spectrum was calculated for all 547 spatial transects and 360, 12-min temporally-indexed sampling periods. The mean global wavelet power was calculated at each spatial and temporal period. Global wavelet power was calculated as a function of period instead of frequency to standardize irregularities in line-transect length. Both wavelet power and scale data were log-normalized, and a best-fit line was regressed using linear least squares for both spatially and temporally-indexed data:

$$\text{Spatial wavelet power} : \log_{10}\left(\frac{\overline{W}_s^2(T_s)}{\delta_s^2}\right) = m_s \times \log_{10}(T_s) + b_s \tag{26}$$

$$\text{Temporal wavelet power} : \log_{10}\left(\frac{\overline{W}_t^2(T_t)}{\delta_t^2}\right) = m_t \times \log_{10}(T_t) + b_t \tag{27}$$

where m and b are the slope and intercept of the best-fit lines. The maximum temporal power spectrum is defined as the power spectrum at the Nyquist frequency:

$$\max(w_t(T)) = m_t \times \log_{10}\left(T_{\frac{1}{2}N(t)}\right) + b_t \tag{28}$$

This equation can be substituted into Eq. 26 to find the spatial scale at which spatial variance matches that observed at the largest temporal scale:

$$\max(w_t(T)) = m_s \times \log_{10}(T_s) + b_s \tag{29}$$

and then solved for T_s to yield the representative spatial scale of the variance $T_{s.\text{rep}}$:

$$T_{s.rep} = 10^{\left(\frac{(\max(w_t(T)) - b_s)}{m_s}\right)} \tag{30}$$

This result is the scale at which an equivalent amount of spatial variability is observed at the maximum temporal scale. High spatial (20 m) and temporal (1.2 s) resolutions are used in the Admiralty Inlet analysis, with both resulting in six acoustic pings per horizontal data bin. The suitability of spatial and temporal resolution choice is checked by calculating the difference in y-intercepts of each log-normalized modeled spectrum.

Optimizing network design for monitoring objectives

Designing monitoring networks includes choice of minimum detectable effect, allowable sampling or interpolation error, and acceptable rate of type I or type II errors. Current sensor networks for MRE monitoring programs are typically designed using resource or logistic constraints (e.g., NYSERDA 2011), without attention to statistical repercussions. The layout and spacing of sensor packages in monitoring networks should be

determined by the sampling requirements needed to meet the network's objectives. One outcome of comparing methods to estimate representative ranges in this study is the ability to modularize network design in a series of objective-driven decisions. The first decision (Fig. 1) is to choose an indicator variable to measure change (e.g., fish density). Once an indicator is chosen, a representative metric is identified to index the quantity through time (e.g. acoustic density). Once the metric is identified, the property of the metric (e.g., mean or variance) is chosen. Historically, declines in the mean of monitoring quantities have been associated with negative effects (Green 1979). Changes in the variance of ecological quantities may affect the health and stability of ecosystems (Underwood 1991; Schindler et al. 2010), making the variance of ecological quantities pertinent metrics of change. The fourth decision is the choice of monitoring approach. Monitoring the mean facilitates detecting change and characterizing distributions. The variability of a quantity can be monitored by determining the spatial-temporal equivalence or by characterizing the spatial variance.

Deciding on the monitoring method used in network design is conditional on previous choices. If detecting change in the mean is the principle objective, then there are three paired *t*-tests/repeated measures ANOVA available to quantify the required number of sensors based on differences between pre- and post-perturbation (e.g., device installation at an MRE site) measurements. The resulting density of instruments is estimated as the number of sensors indicated by the representative range, divided by the site area. Of the three paired *t*-test based choices, the power analysis method includes information on statistical power, resolvable effect size, and prevalence of false positives. If the monitoring objective is to map the distribution of a monitoring metric, then the spatial autocorrelation approach quantifies spacing between sensors. Either the lagged correlation coefficient or lagged coefficient of determination can be used to estimate a representative range, but a threshold of what constitutes "representative" needs to be defined. The coefficient of determination is recommended as an index due to its straightforward interpretation as the proportion of

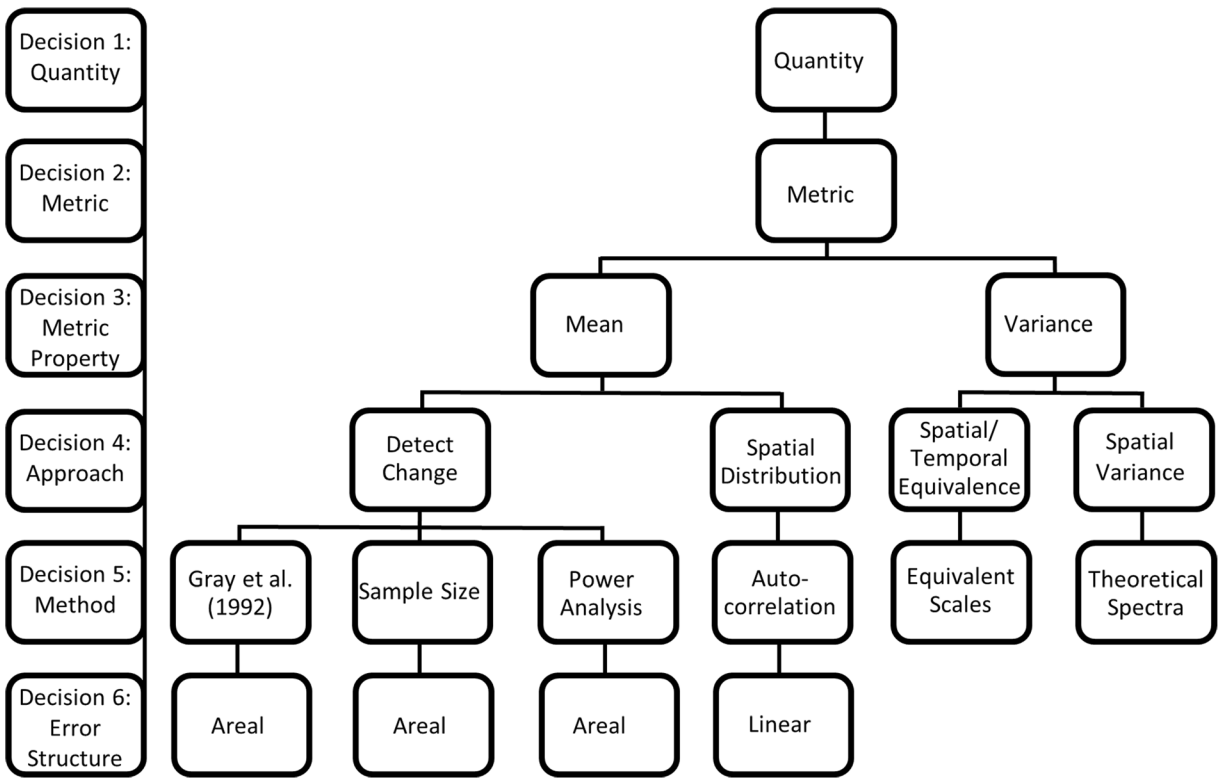

Fig. 1 Decision tree for the design of distributed monitoring networks. Six questions are used to determine a monitoring metric and the corresponding method to calculate representative range (see text for question detail)

explained variance. Unlike previous studies that used significant deviations from a perfect correlation as a benchmark for representative (e.g., Jacobs 1989), this study used the range at which observations became statistically independent as the criterion to determine representative range. Once the representative range is determined, then an interpolation error at any point can be estimated as a function of range (e.g., linear or aerial), which increases the understanding of uncertainty in spatial models of the monitored quantity. If the network design objective is to monitor variance of a quantity within a domain, then the theoretical spatial spectra should be used to place sensors at the spatial periodicity that will maximize observed variance. And finally, if the network design objective is to interpolate temporal variability over space, then the equivalent periods of variance method should be used. A primary difference between mean and variance methods is that variance methods identify the period at which measurements can be considered equivalent. Neither variance method calculates statistical power.

This approach enables the design of a distributed monitoring network in a set of six decisions. The six methods used to estimate representative ranges are demonstrated using fish density at a MRE tidal turbine site, but we advocate that this approach can be applied to any aquatic or terrestrial, distributed network. Static sensor networks provide high-scope, spatiotemporal data that quantify ecological pattern and increase understanding of relevant environmental processes across spatial and temporal scales. Optimizing these networks to meet objectives will help manage network expectations, increase network performance, increase cost-efficacy, and simplify network design. Importantly, this approach also provides tools for ecologists and engineers to quantify error introduced by spatially interpolating point measurements and to document the rationale used in static sensor network design decisions.

Admiralty Inlet case study

Admiralty Inlet is the site of the Snohomish Public Utility District 1 (SnoPUD) tidal energy pilot project that received its project license from the Federal Energy Regulatory Commission (FERC) on March 20, 2014. The site is dynamic, with an average tidal current speed of 1.4 m s^{-1} and maximum speeds reaching almost 3 m s^{-1}. The project, now dormant, would deploy two, 6 m OpenHydro turbines (http://www.openhydro.com) approximately 1 km west of Admiralty Head, Puget Sound Washington (48.18° N, 122.73° W), at a depth of approximately 55 m with two sub-sea power cables connecting the turbines to the onshore electric grid.

Mobile and stationary acoustic surveys

To estimate representative ranges, concurrent spatially- and temporally-indexed data are needed. Mobile, surface acoustic surveys were used to collect spatially-indexed data, while a stationary, bottom-deployed echosounder collected temporally-indexed data. For surface surveys, an 8 km^2 grid of six high- (0.25 km) and six low- (0.5 km) resolution, parallel surface transects encompassed the proposed location of the tidal turbines. Mobile acoustic surveys were repeated from May 2 to May 13 and again from June 3 to June 14, 2011. A 120 kHz Simrad EK60 echosounder with a hull-mounted transducer was used to measure reflected energy or mean volume backscattering strength (S_v units dB re 1 m^{-1}; MacLennan et al. 2002). Acoustic backscatter is representative of nekton (i.e., macro-invertebrates and fish that move independently of fluid motion) density in the water column. The transducer, with a transmit power of 500 W, had a beam width of 7° (between half power points). Nekton density was sampled using a pulse duration of 0.512 ms at 1 Hz. The echosounder was calibrated using a 38.1 mm tungsten-carbide sphere following protocols of Foote et al. (1987).

Temporally-indexed, acoustic backscatter data was measured using an upward-looking, 120 kHz BioSonics DTX echosounder (http://www.biosonicsinc.com/product-dtx-portable-echosounder.asp) mounted on a Sea Spider (http://www.oceanscience.com/Products/Seafloor-Platforms/Sea-Spiders.aspx) fiberglass platform that was deployed in 55 m of water at a distance of approximately 750 m from Admiralty Head. The echosounder sampled using a 100 W, 0.5 ms pulse at 5 Hz for 12 min every 2 h through a factory calibrated, 7° beam (between half power points) transducer.

Acoustic data processing

Acoustic data were processed using Echoview (v.5.4.91, http:\\www.echoview.com) software. Mobile acoustic measurements were analyzed between 3 m of the transducer face and a half meter from the bottom to avoid transceiver saturation, the acoustic nearfield, and backscatter from the bottom. Backscatter from mobile

survey measurements was dominated by turbulence introduced by tidal currents, sometimes extending from the surface to more than 80 m depth. Turbulence was identified and excluded from analysis using Echoview's school detection algorithm (minimum total school length = 5 m, minimum total school height = 3 m, minimum candidate length = 5 m, minimum candidate height = 3 m, maximum vertical linking distance = 10 m, maximum horizontal linking distance = 10 m). Detected schools that intersected the 3 m surface exclusion region were classified as surface turbulence and excluded from further analysis. Echosounder data were exported at a − 75-dB re 1-m^{-1} (hereafter dB) threshold and a 16 dB signal-to-noise ratio, to enhance the exclusion of turbulence.

Stationary acoustic measurements were limited to a range of 3 to 26 m from the transducer face, corresponding to twice the vertical footprint of the proposed OpenHydro turbines. Stationary backscatter measurements were exported using a − 75 dB threshold, identical to that of the mobile survey backscatter measurements. Cells that failed to meet the 16 dB signal-to-noise ratio were excluded from further analysis.

Correlation coefficients, lagged in space or time, were used to determine the spatial or temporal resolution at which mobile or stationary backscatter measurements of nekton density were independent. Horizontal autocorrelation of vertically integrated (i.e., summed) mean volume backscattering strength (i.e., S_v units dB re 1 m^{-1}) was used to determine the range at which measurements became statistically independent. These ranges were used as the horizontal resolution of the spatially and temporally-indexed data. Once mobile and stationary horizontal resolutions were determined, mean S_v was exported in 1 m vertical bins.

Characterizing vertical density distributions

Data from the 1 m vertical cells were used to derive four metrics to characterize vertical distribution of nekton density within each horizontal cell: mean volume backscattering strength (mean S_v), center of mass (CM), inertia (I), and an aggregation index (AI). Mean volume backscattering strength is a depth-independent metric of density through the water column. The remaining three metrics were selected from a suite of metrics developed by Burgos and Horne (2007) and refined by Urmy et al. (2012) to summarize the vertical distribution of nekton. Center of mass (units: m) is the mean weighted location of backscatter in the water column relative to the bottom. Inertia (units: m^2) measures dispersion and is analogous to the variance of the center of mass. The aggregation index (units: m^{-1}) measures the vertical patchiness of backscatter through the water column calculated on a scale of 0 to 1, with 1 being aggregated.

Results

Representative range of the mean

Spatial autocorrelation

Spatial autocorrelation of nekton density measurements decayed as a function of distance (Fig. 2). Exponential decay models were fit to the lagged Pearson's correlation coefficient ($\rho(h) = 0.803e^{-01.87d}$) and lagged coefficient of determination ($\rho(h) = 0.3392e^{-0.168d}$) models.

The y-intercept of the lagged coefficient of determination model at lag 1 $\rho(1) = 0.286$ demonstrates that less than a third of the variability between sequential observations can be explained by autocorrelation. Because correlation coefficients were calculated for each transect, the median length transect was used to calculate a threshold for significance (i.e., 2600 m transect sampled at a 20-m resolution, yielding $l = 130$ samples). The corresponding length of the 95% confidence interval for a lagged, correlation coefficient at the median transect length is 0.175 and 0.0307 for the coefficient of determination. These thresholds correspond to the range at which observations approach independence. A threshold of 0.0307 results in a representative range of 285.65 m in Admiralty Inlet. Given a circle with a radius of 285.65 m, an instrument density of 3.82 sensors km^{-2} is required to monitor the domain (Table 2).

Sample size and power analysis calculations

The mean representative range using the Gray et al. (1992) formula (Eq. 8) is 403.9 m (Fig. 3a), and the statistically-derived sample size calculation from Eq. 15 yields a representative mean range of 30.57 m (Fig. 3b). The power analysis using $\alpha = 0.05$ and $\beta = 0.90$ (Eq. 16) results in a mean representative range of 88.45 m (Fig. 3c). Representative mean ranges of 403.9, 30.57, and 88.45 m correspond to sensor densities of 1.95, 340.6, and 40.68 sensors km^{-2} (Table 2).

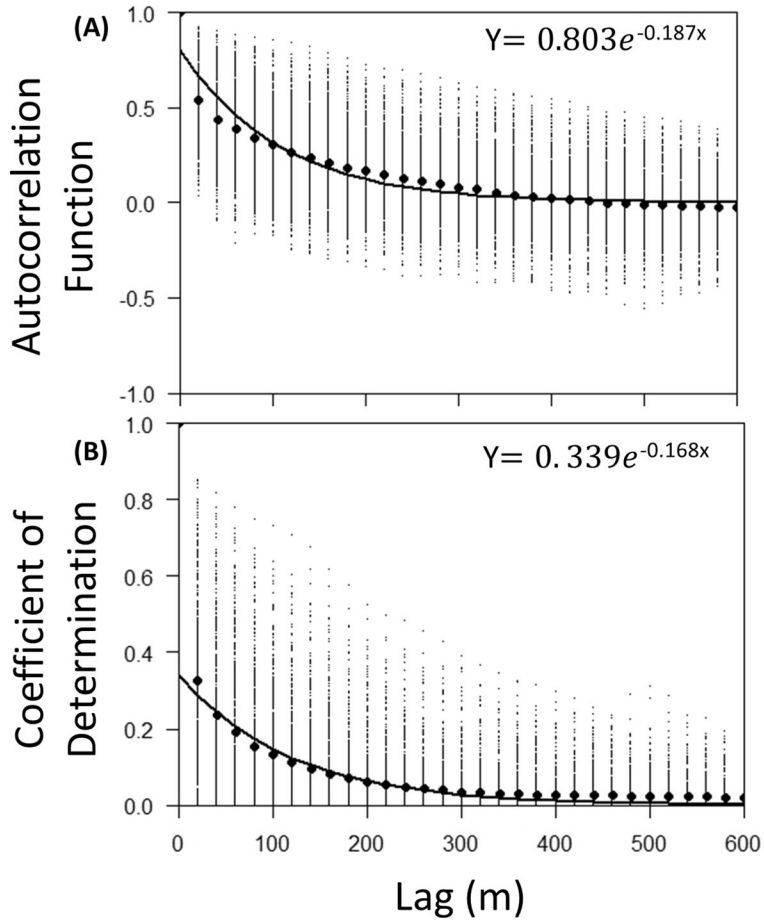

Fig. 2 Spatial autocorrelation of acoustic backscatter measurements as a function of distance. Large black points denote the mean **a** autocorrelation coefficient or **b** coefficient of determination across all 547 transects at each lag distance. Individual correlation values for each transect are plotted as small points

Representative range estimates are dependent on the statistical power used to detect temporal deviations. Setting $\alpha = 0.05$ and the effect size $E = 1$ dB constant, the representative range increases 30% from 88.45 m to 115.41 m when β decreases from 0.9 to 0.7 (Fig. 4). This increase is smaller than the standard deviation of

Table 2 Estimated representative ranges, instrument density, and estimated monitoring costs per square kilometer. Instrument density is calculated using the representative range as the radius of a circular area. Costs are based on a $75,000 USD instrument package and an Admiralty Inlet site area of 0.09 km^2

Method	Representative range (m)	Instrument density (no. km^{-2})	Density cost ($ km^{-2})	Admiralty Inlet cost ($)
Coefficient of determination	288.65	3.82	286,529	75,000
Gray's sample size	403.90	1.95	146,340	75,000
T test sample size	30.57	340.61	25,545,859	2,325,000
Power analysis	88.45	40.69	3,051,516	300,000
Theoretical spectra	1388.10	0.17	12,390	75,000
Corresponding spatial and temporal scales	648.70	0.76	56,731	75,000

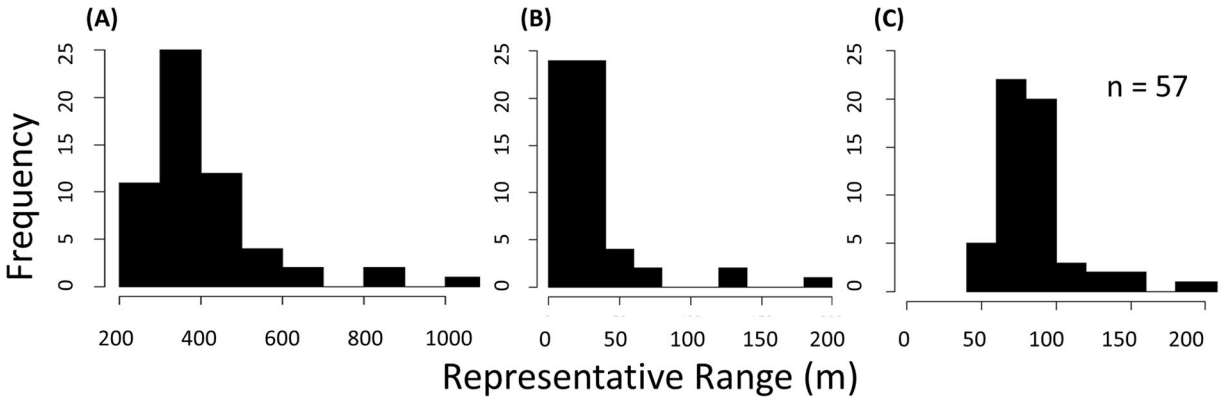

Fig. 3 Frequency distributions of acoustic backscatter representative ranges calculated for each sampling grid required to identify a 1 dB change from **a** the Gray et al. (1992) formula, **b** sample size calculation to identify mean paired differences, and **c** a power analysis with $\alpha = 0.05$ and $\beta = 0.90$

independently calculated representative ranges ($\alpha = 0.05$, $\beta = 0.90$) for each sampling grid ($\sigma = 36.17$ sensors, $n = 57$). If β is held constant at 0.90 and α is increased from 0.05 to 0.1, then the representative range increases from 88.45 to 97.98 m. To depict potential uncertainty in the representative range estimates, a one standard deviation from the mean is shown in Fig. 4 at $\alpha = 0.05$. The uncertainty envelope increases as the β value decreases.

Relative standard interpolation error

Interpolating point measurements of fish density potentially introduces errors (Fig. 5a). The absolute interpolation error, analogous to the standard deviation surrounding the interpolated estimate, is 2.93 dB at the shortest representative range of 30.57 m (i.e., paired *t*-test difference). Since decibels are a logarithmic ratio, a value ± 2.93 dB equates to a potential 96% increase or a 49.93% decrease in fish density at the interpolated point. The next smallest representative range, calculated using power analysis, results in an interpolation error of 3.44 dB (+ 120% or − 54.7%) at a range of 84.45 m. Differences in interpolation error between the larger two representative ranges, 285.65 and 403.9 m, are proportionately small compared to the interpolation error at shorter representative ranges. The interpolation error stabilizes and asymptotically approaches the average standard deviation, 4.32 dB, at ranges greater than approximately 450 m.

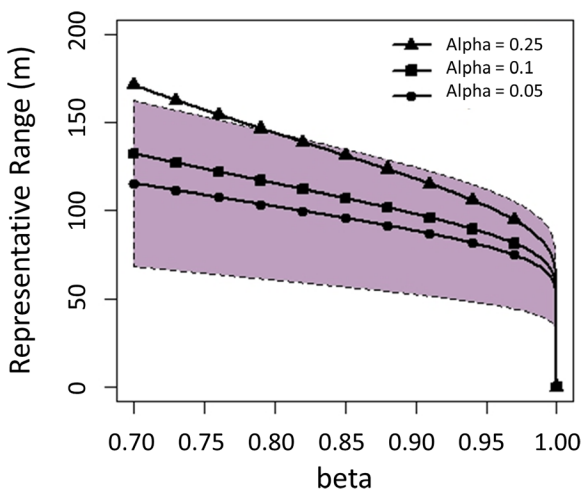

Fig. 4 Representative ranges of mean backscatter density from surface acoustic grid surveys ($n = 57$) calculated using three α values (0.25, 0.1, 0.05) from paired *t*-test, power analyses. The polygon envelops the mean range at $\alpha = 0.05 \pm$ one standard deviation

Areal interpolation errors increase following a power function (Fig. 5b). The error when estimating fish density over an area defined by a representative range of 30.57 m (2.9×10^{-3} km^2) is 2.4 dB (i.e., an increase of 73.8%), which increases to 3.69 dB (+ 133.88%) over an area defined by a range of 88.45 m. The interpolation error further increases to 6.37 dB (+ 333.5%) within the area defined by a radius of 285.65 m and to 7.53 dB (+ 466.2%) at a range of 403.9 m.

Representative ranges of variance

The relative variance modeled from the first-order autocorrelation of fish densities asymptotically approaches a maximum value of 4.98 times the white-noise variance over infinite periods. The scale at which 95% of the maximum variance, 4.74, is measured was considered the representative scale of the variance. The relative variance exceeds the 95% maximum threshold at a

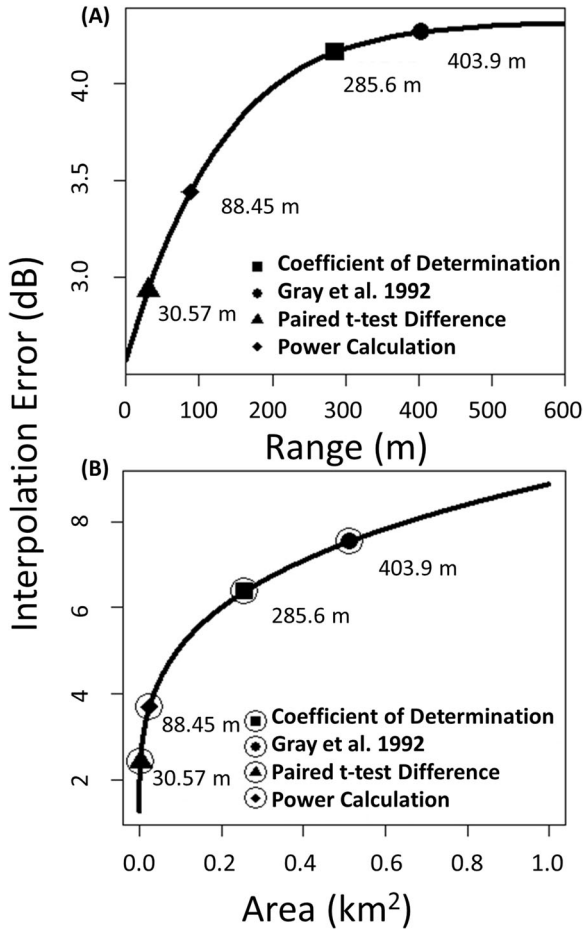

Fig. 5 Interpolation errors of **a** backscatter point measurements to spatially discreet points and **b** backscatter point measurements to representative areas. The representative ranges of the mean for each algorithm are marked for the linear distance and the radius of a circle (see Table 2)

period of 1338 m (Fig. 6 and Table 2). Data analyzed over larger periods than 1338 m would see negligible increases in variance.

As expected, spatial and temporal spectral power increases with period (Fig. 7). The *y*-intercepts from both spatial and temporal spectra are nearly identical (0.34 and 0.33 $\log_{10}(dB^2)$), strengthening the supposition that spatial and temporal resolutions are comparable. Since there is no equivalence between spatial and temporal units, it is not possible to statistically test differences between the two spectra. Ordinate units were set relative to the 20 m and 1.2 s resolutions of the spatial and temporal surveys. At these resolutions, the spatial spectra ($Y = 0.34 + 0.777x$) increase more rapidly than the temporal spectra ($Y = 0.33 + 0.478x$). The modeled maximum temporal variance at the Nyquist frequency, equivalent to a period of 6 min, is 1.51 $\log_{10}(dB^2)$. The corresponding amount of spatial

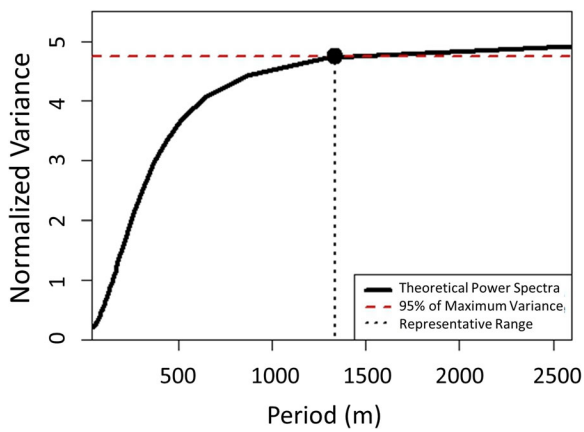

Fig. 6 A first-order, auto-regressive, theoretical power spectra of fish density. The representative range of the variance is arbitrarily set to the period corresponding to 95% of the maximum expected variance

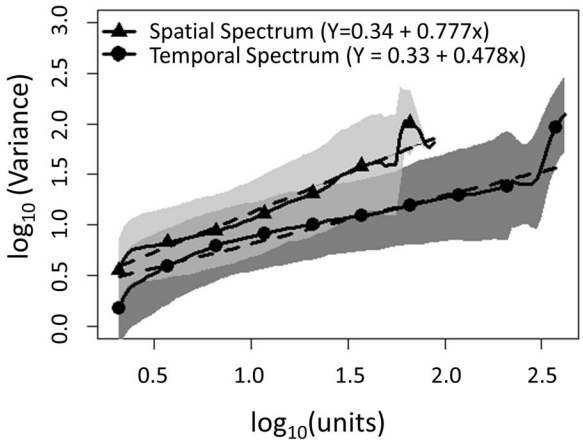

Fig. 7 Spatial (diamond) and temporal (circle) power spectra, calculated using the global wavelet spectrum. Spatial and temporal data units on the x-axis correspond to spatial and temporal resolutions of 20 m and 1.2 s. The dashed line in each plot is the modeled log-normalized spectrum with the corresponding equation noted in the legend. The representative range is the spatial period (648.7 m) with identical magnitudes of temporal variance

variability occurs at a period of 648.7 m, which is interpreted as the representative range (Table 2). An approximately equal amount of variance is observed within the calculated 547 spatial and 360 temporal spectra, as denoted by standard deviation envelopes.

Summary of representative ranges

The representative spatial range of static temporal sensors is dependent on the quantity measured, the derivation method, and associated assumptions. Among the four methods used to quantify representative range of mean fish density, values range from 30.6 to 403.9 m. Representative ranges of the variance are 648.7 and 1388.1 m (Table 2). When representative ranges are used as radii to calculate representative circular areas, complete coverage requires a minimum of 1.95 to 340.61 sensors per square kilometer. Sensor densities measuring the mean are higher than those needed to monitor the variance, suggesting that networks designed to measure the mean of a quantity (e.g., fish density) will have adequate spatial coverage to also characterize the variance.

Discussion

Comparison of methods

The six methods used to calculate representative ranges vary in their assumptions and resulting estimates. The four methods used to quantify representative ranges of a mean assume a random sampling pattern, which ignores additional information from spatial autocorrelation measures. The random sampling methods do not use multiple control sites that are needed to detect change from an initial condition (Skalski and McKenzie 1982; Underwood 1994) but provide an example of how to calculate representative range for paired *t*- test/ANOVA-based sampling approaches. The spatial autocorrelation method identifies the range at which measurements become statistically independent, assuming that as spatial autocorrelation approaches zero, measurements become statistically independent. Spatial autocorrelation is dependent on the location, resolution, and spatial extent of the data (Ciach and Krajewski 2006; Ciannelli et al. 2008). In systems where variance increases with range (e.g., spatial drift, gradient; Wiens 1989), the representative range will increase as the survey area is expanded. Therefore, the domain of a network must be delineated before the representative range can be used for network design.

Matching temporal to spatial variance scales assumes that temporal and spatial variances are equivalent. Links between spatial periods of physical processes and temporal scales have been demonstrated (e.g., Steele et al. 1994; Wu 1999), including scale-dependent differences in the autocorrelation of rainfall (Ciach and Krajewski 2006). Wiens (1989) noted that long-term studies conducted over small spatial scales have low predictive power, whereas studies covering large spatial extents over short temporal periods have high pseudo-predictability, as repeated samples typically have short temporal sampling intervals. The importance of analyzing spatiotemporal data at equivalent spatial and temporal scales has been emphasized (Wiens 1989), but there remains a lack of methods to accomplish this task. Quantifying the relationship between spatial and temporal variance spectra provides one approach.

The six methods used to estimate representative ranges are not exhaustive but represent those available for *a priori* network design using data from baseline samples. *A posteriori* methods to optimize the density of established networks exist (e.g., Sulkava et al. 2011) but are limited to network optimization. Evaluating *a posteriori* methods is beyond the scope of this study but should be used during operations to test network performance and to optimize the spatial allocation of sampling effort. As an example, Janis and Robeson (2004) identify instances when a network could not be considered representative based on the magnitude of

variability at resolutions coarser than that of the network (i.e., analogous to the nugget effect).

Biological monitoring at Marine Renewable Energy sites

Monitoring programs at MRE sites represent a large portion of pilot site development costs (e.g., NYSERDA 2011) and contribute to both operating and decommissioning costs during the life cycle of all MRE projects. Biological monitoring at MRE sites should be as efficient and cost-effective as possible. Stationary sensor networks are assumed to be more cost-effective than repeated, mobile surveys due to labor, fuel, and vessel operation costs. Still, the cost of static monitoring networks may be unnecessarily increased by the environmental precautionary principle (Underwood 1997; Underwood and Chapman 2003), where any "error" or uncertainty in survey design should favor environmental protection and will inflate costs of implementation. Quantifying the representative range and the spatial interpolation error removes uncertainty in the monitoring network design and reduces monitoring costs by identifying the minimum number of sensor packages for complete coverage of the site. Depending on the spatial extent of the network and the cost of purchasing, deploying, retrieving, and analyzing data from sensors, representative ranges estimated in this study should reduce costs compared to the ad hoc network designs of current MRE biological monitoring programs.

The density of sensor packages within a monitoring network potentially affects the economic feasibility of expanding pilot (i.e., 100 m^2) to commercial (i.e., 10 km^2) scale MRE sites. Using an estimated cost of $75,000 for an acoustic monitoring package (e.g., NYSERDA 2011, Verdant Power 2010a), the proposed Admiralty Inlet tidal turbine site (area = 0.09 km^2) would require 31 monitoring packages using the most conservative *t*-test sample approach, 4 using the power analysis, and 1 using the Gray et al. (1992) or the Anttila et al. (2008) methods. This range represents a cost difference $2.25 million USD to monitor the Admiralty Inlet site (Table 2). As a comparison, the Roosevelt Island Tidal Energy project in East River New York deployed an array of 24 acoustic transducers (NYSERDA 2011) to monitor a 0.086-km^2 site (FERC 2012), as a component of a $2.35 million monitoring plan that costs an additional $340,000 annually for operations and maintenance (Verdant Power 2010b). The site area and number of sensors used in monitoring the Roosevelt Island Tidal Energy project translate to a representative range of 33.77 m, consistent with the most conservative representative range estimated for Admiralty Inlet. When pilot projects are scaled to commercial operations, differences in monitoring costs will be further amplified depending on the choice of metric property (i.e., mean or variance) and the method used to calculate representative range.

Acknowledgements This study was made possible by the US National Oceanographic Partnership Program, the Bureau of Ocean Energy Management (M10PC00093), and the National Science Foundations' Sustainable Energy Pathways Program (CHE-1230426). Pierre Petigas suggested the rain gauge analogy. Three anonymous reviewers are thanked for comments that increased clarity of the paper.

References

Anttila, S., Kairesalo, T., & Pellikka, P. (2008). A feasible method to assess inaccuracy caused by patchiness in water quality monitoring. *Environmental Monitoring Assessment, 142*(1), 11–22.

Bence, J. R. (1995). Analysis of short time series: correcting for autocorrelation. *Ecology, 76*(2), 628–639.

Brooks, C. F. (1947). Recommended climatological networks based on the representativeness of climatic stations for different elements. *Transactions of the American Geophysical Union, 28*(6), 845–846.

Burgos, J. M., & Horne, J. K. (2007). Sensitivity analysis and parameter selection for detecting aggregations in acoustic data. *ICES Journal of Marine Science, 64*(1), 160–168.

Certain, G., Bellier, E., Planque, B., & Bretagnolle, V. (2007). Characterizing the temporal variability of the spatial distribution of animals: an application to seabirds at sea. *Ecography, 30*(5), 695–708.

Ciach, G. J., & Krajewski, W. F. (2006). Analysis and modeling of spatial correlation structure in small-scale rainfall in central Oklahoma. *Advances in Water Resources, 29*(10), 1450–1463.

Ciannelli, L., Fauchald, P., Chan, K. S., Agostini, V. N., & Dingsør, G. E. (2008). Spatial fisheries ecology: recent progress and future prospects. *Journal of Marine Systems, 71*(3–4), 223–236.

Damian, D., Sampson, P. D., & Guttorp, P. (2003). Variance modeling for nonstationary spatial processes with temporal replications. *Journal of Geophysical Research – Atmospheres, 108*(D24), 8778.

Ellis, J. I., & Schneider, D. C. (1997). Evaluation of a gradient sampling design for environmental impact assessment. *Environmental Monitoring and Assessment, 48*(2), 157–172.

FERC (Federal Energy Regulatory Commission). (2012). *Order issuing pilot project license: Verdant Power, LLC.* Project No. 12611-005.

Foote, K.G., Knudsen, H.P., Vestnes, G., MacLennan, D.N., Simmonds, E.J. (1987). Calibration of acoustic instruments

for fish density estimation: a practical guide. *ICES Cooperative Research Report No*. 144.

Gandin, L.S. (1970). The planning of meteorological station networks. *World Meteorological Organization Technical Note* No. 111, Geneva.

Garcillán, P. P., & Ezcurra, E. (2003). Biogeographic regions and ß-diversity of woody dryland legumes in the Baja California peninsula. *Journal of Vegetation Science, 14*(6), 859–868.

Gilman, D. L., Fuglister, F. J., & Mitchell Jr., J. M. (1962). On the power spectrum of "red noise". *Journal of Atmospheric Science, 20*(2), 182–184.

Godø, O. R., Handegard, N. O., Browman, H. I., Macaulay, G. J., Kaartvedt, S., & Giske, J., et al. (2014). Marine ecosystem acoustics (MEA): quantifying processes in the sea at the spatio-temporal scales on which they occur. *ICES Journal of Marine Science, 71*(8), 2357–2369.

Gray, J. S., McIntyre, A. D., Stim, J. (1992). Biological assessment of marine pollution—with particular reference to benthos. *FAO Technical Paper No. 324: Manual of Methods in Aquatic Environment Research*. Rome.

Green, R. H. (1979). *Sampling design and statistical methods for environmental biologists*. Chichester: Wiley.

Hershfield, D. M. (1965). On the spacing of rain gauges. *Symposium Design of Hydrological Networks no. 67 of I.A.S.H.*

Hocke, K., & Kämpfer, N. (2011). Hovmöller diagrams of climate anomalies in NCEP/NCAR reanalysis from 1948 to 2009. *Climate Dynamics, 36*(1–2), 355–364.

Hubbell, S. P. (2001). *The unified neutral theory of biodiversity and biogeography*. Princeton: Princeton University Press.

Hudgins, L., Friehe, C. A., & Mayer, M. E. (1993). Wavelet transforms and atmospheric turbulence. *Physical Review Letters, 71*(20), 3279–3282.

Huff, F. A., Neill, J. C. (1957). Rainfall relations on small areas in Illinois. *Bulletin of Illinois State Water Service no. 44*.

Hutchinson, P. (1969). Estimation of rainfall in sparsely gauged areas. *Hydrological Sciences Journal, 14*(1), 101–119.

Hutchinson, P. (1970). A contribution to the problem of spacing raingauges in rugged terrain. *Journal of Hydrology, 12*(1), 1–14.

Jacobs, J. D. (1989). Spatial representativeness of climatic data from Baffin Island, NWT, with implications for muskoxen and caribou distribution. *Arctic, 42*(1), 50–56.

Janis, M., & Robeson, S. (2004). Determining the spatial representativeness of air-temperature records using variogram-nugget time series. *Physical Geography, 25*(6), 513–530.

Kagan, R. L. (1966). An evaluation of representativeness of precipitation data. *Works of the Main Geophysical Observatory*. USSR. Vol. 191.

Kagan, R. L. (1972). Precipitation – Statistical Principles. In WMO Publication No. 324, *The Casebook on Hydrological Network Design Practice*. World Meteorological Organization, Geneva.

Kitsiou, D., Tsirtsis, G., & Karydis, M. (2001). Developing an optimal sampling design. A case study in a coastal marine ecosystem. *Environmental Monitoring Assessment, 71*(1), 1–12.

Legendre, P. (1993). Spatial autocorrelation: trouble or new paradigm? *Ecology, 74*(6), 1659–1673.

Liu, Y., San Liang, X., & Weisberg, R. H. (2007). Rectification of the bias in the wavelet power spectrum. *Journal of Atmospheric and Oceanic Technology, 24*(12), 2093–2102.

MacLennan, D. N., Fernandes, P. G., & Dalen, J. (2002). A consistent approach to definitions and symbols in fisheries acoustics. *ICES Journal of Marine Science, 59*(2), 365–369.

Martin, A. P., Zubkov, M. V., Burkill, P. H., & Holland, R. J. (2005). Extreme spatial variability in marine picoplankton and its consequences for interpreting Eulerian time-series. *Biology Letters, 1*(3), 366–369.

Milewska, E., & Hogg, W. D. (2001). Spatial representativeness of a long-term climate network in Canada. *Atmosphere-Ocean, 39*(2), 145–161.

Mønness, E., & Coleman, S. (2011). *A short note on variograms and correlograms*. Notat nr. 1-2011. Hedmark University College.

Nekola, J. C., & White, P. S. (1999). The distance decay in biogeography and ecology. *Journal of Biogeography, 26*(4), 867–878.

NYSERDA (New York State Energy Research and Development Authority). (2011). *Roosevelt Island Tidal Energy (RITE) Environmental Assessment Project*. NYSERDA 9892-1. Albany, New York.

Percival, D. P. (1995). On estimation of the wavelet variance. *Biometrika, 82*(3), 619–631.

Perrier, V., Philipovitch, T., & Basdevant, C. (1995). Wavelet spectra compared to Fourier spectra. *Journal of Mathematical Physics, 36*(3), 1506–1519.

Platt, T., & Denman, K. L. (1975). Spectral analysis in ecology. *Annual Review of Ecology and Systematics, 6*, 189–210.

Porter, J., Arzberger, P., Braun, H.-W., Bryant, P., Gage, S., Hansen, T., et al. (2005). Wireless sensor networks for ecology. *Bioscience, 55*(7), 561–572.

Posadas, P., Crisci, J. V., & Katinas, L. (2006). Historical biogeography: a review of its basic concepts and critical issues. *Journal of Arid Environments, 66*(3), 389–403.

Verdant Power. (2010a). *Roosevelt Island Tidal Energy Project (FERC No. 12611): Final Kinetic Hydrokinetic Pilot License Application,* Volume 4, Part 1 of 3. Verdant Power, LLC, New York.

Verdant Power. (2010b). *Roosevelt Island Tidal Energy Project (FERC No. 12611): Final Kinetic Hydropower Pilot License Application*, Volume 2, Part 2 of 2. Verdant Power, LLC, New York.

Rhodes, J. R., & Jonzén, N. (2011). Monitoring temporal trends in spatially structured populations: how should sampling effort be allocated between space and time? *Ecography, 34*(6), 1040–1048.

Roughgarden, J. (1977). Patchiness in the spatial distribution of a population caused by stochastic fluctuations in resources. *Oikos, 29*(1), 52–59.

Rycroft, H. B. (1949). Random sampling of rainfall. *Journal of the South African Forestry Association, 18*(1), 71–81.

Sampson, P., Damian, D., Guttorp, P. (2001). Advances in modelling and inference for environmental processes with nonstationary spatial covariance. In Allard, D., Monestiez, P., Froidevaux, R. (eds), GeoENV2000: *Third European Conference on Geostatistics for Environmental Applications*.

Schindler, D. E., Hilborn, R., Chasco, B., Boatright, C. P., Quinn, T. P., Rogers, L. A., et al. (2010). Population diversity and the

portfolio effect in an exploited species. *Nature, 465*(7298), 609–612.

Schneider, D. C. (1990). Spatial autocorrelation in marine birds. *Polar Research, 8*(1), 89–97.

Siljamo, P., Sofiev, M., Ranta, H., Linkosalo, T., Kubin, E., Ahas, R., et al. (2008). Representativeness of point-wise phenological *Betula* data collected in different parts of Europe. *Global Ecology and Biogeography, 17*(4), 489–502.

Skalski, J. R., & McKenzie, D. H. (1982). A design for aquatic monitoring programs. *Journal of Environmental Management, 14*(3), 237–251.

Soininen, J., McDonald, R., & Hillebrand, H. (2007). The distance decay of similarity in ecological communities. *Ecography, 30*(1), 3–12.

Steele, J. H., Henderson, E. W., Mangel, M., & Clark, C. (1994). Coupling between physical and biological scales. *Philosophical Transactions of the Royal Society London B, 343*(1303), 5–9.

Sulkava, M., Luyssaert, S., Zaehle, S., & Papale, D. (2011). Assessing and improving the representativeness of monitoring networks: the European flux tower network example. *Journal of Geophysical Research, 116*(G3), G00J04.

Sullivan, L. M. (2006). Estimation from samples. *Circulation, 114*(5), 445–449.

Torrence, C., & Compo, G. P. (1998). A practical guide to wavelet analysis. *Bulletin of the American Meteorological Society, 79*(1), 61–78.

Tversky, A., & Kahneman, D. (1975). Judgement under uncertainty: heuristics and biases. In D. Wendt & C. Vlek (Eds.), *Utility, probability, and human decision making* (pp. 141–162). Reidel: Boston.

Underwood, A. J. (1991). Beyond BACI: experimental designs for detecting human environmental impacts on temporal variations in natural populations. *Marine and Freshwater Research, 42*(5), 569–587.

Underwood, A. J. (1994). On beyond BACI: sampling designs that might reliably detect environmental disturbances. *Ecological Applications, 4*(1), 4–15.

Underwood, A. J. (1997). Environmental decision-making and the precautionary principle: what does this principle mean in environmental sampling practice? *Landscape and Urban Planning, 37*(3–4), 137–146.

Underwood, A. J., & Chapman, M. G. (2003). Power, precaution, type II error and sampling design in assessment of environmental impacts. *Journal of Experimental Marine Biology and Ecology, 296*(1), 49–70.

Urmy, S. S., Horne, J. K., & Barbee, D. H. (2012). Measuring the vertical distributional variability of pelagic fauna in Monterey Bay. *ICES Journal of Marine Science, 69*(2), 184–196.

Wiens, J. A. (1976). Population responses to patchy environments. *Annual Review of Ecology and Systematics, 7*, 81–120.

Wiens, J. A. (1989). Spatial scaling in ecology. *Functional Ecology, 3*(4), 385–397.

Wu, J. (1999). Hierarchy and scaling: extrapolating information along a scaling ladder. *Canadian Journal of Remote Sensing, 25*(4), 367–380.

Zar, J. H. (2010). *Biostatistical analysis* (5th ed.). Pearson: Upper Saddle River, New Jersey.